

# Diagnosis of Thin-Cap Fibroatheromas by a Self-Contained Intravascular Magnetic Resonance Imaging Probe in Ex Vivo Human Aortas and In Situ Coronary Arteries

Jacob Schneiderman, MD,\* Robert L. Wilensky, MD, FACC,† Assaf Weiss, BSc,‡ Eitzek Samouha, BSc,‡ Lev Muchnik, BSc,‡ Malca Chen-Zion, PhD,‡ Mordechai Ilovitch, PhD,‡ Erez Golan, MSc,‡ Aharon Blank, PhD,‡ Moshe Flugelman, MD,§ Yosef Rozenman, MD, FACC,|| Renu Virmani, MD, FACC¶

Tel Aviv, Lod, Haifa, and Holon, Israel; Philadelphia, Pennsylvania; and Washington, DC

<b>OBJECTIVES</b>	We sought to correlate findings obtained from a self-contained magnetic resonance imaging (MRI) probe with plaque morphology of ex vivo human aortas and coronary arteries.
<b>BACKGROUND</b>	Early detection of thin-cap fibroatheromas (TCFAs) may allow for early preventive treatment of acute coronary syndromes. We developed an intravascular MRI catheter capable of imaging the arterial wall without external magnets or coils by differentiating lipid-rich and fibrotic-rich areas of the atherosclerotic plaque on the basis of differential water diffusion.
<b>METHODS</b>	Aortic samples (n = 16) and coronary arteries were obtained within 12 h of death. Coronary specimens were intermediate in angiographic severity (30% to 60% luminal narrowing, n = 18). Blinded histologic and immunohistochemical analyses of the tissues were performed and correlated to MRI findings.
<b>RESULTS</b>	The 16 aortic lesions included four ulcerated plaques, two TCFAs, two thick-cap fibrous atheromas, two intimal xanthomas, and six adaptive intimal thickenings. The MRI scan correctly correlated with the histologic diagnosis in 15 (94%) of 16 lesions. The 18 coronary lesions included one plaque rupture, three TCFAs, seven thick-cap fibrous atheromas, four fibrocalcific plaques, two intimal xanthomas, and one adaptive intimal thickening. The MRI scan correlated with the histologic diagnosis in 16 of 18 lesions (sensitivity 100%, specificity 89%).
<b>CONCLUSIONS</b>	The self-contained intravascular MRI catheter successfully identified TCFA and may prove to be an important diagnostic approach to determining the presence of lesions with increased risk of causing death or myocardial infarction. (J Am Coll Cardiol 2005;45:1961-9) © 2005 by the American College of Cardiology Foundation

Coronary plaque rupture with subsequent thrombus formation is the underlying cause of the majority of acute coronary syndromes (1,2). The conversion of an inactive plaque into an unstable, rupture-prone lesion is linked to the interplay between the fibrous cap thickness, necrotic core size, and

See page 1970

extent of macrophage infiltration (3,4). A thin fibrous cap covering a large necrotic core is the morphologic characteristic indicative of thin-cap fibroatheroma (TCFA), considered to be a vulnerable plaque. Early diagnosis of TCFAs may lead to more aggressive treatment of symptomatic and

asymptomatic coronary artery disease in order to reduce the incidence of death and myocardial infarction (5-9).

Magnetic resonance imaging (MRI) provides detailed tissue characterization of aortic and carotid atherosclerotic plaques and has identified carotid plaques that cause symptoms (10). However, it is difficult to apply MRI to coronary lesions due to cardiac motion caused by myocardial contraction and respiration (11). In addition, the need for external magnets has made MRI evaluations within the catheterization laboratory impractical.

Using MRI combined with pulsed field gradient methods, Toussaint et al. (12) calculated the apparent water diffusion coefficient (ADC) of various components of the atherosclerotic vascular wall. Their results showed decreased and isotropic water diffusion within the atherosclerotic plaque, compared with the fibrous cap and medial smooth muscle layer, a finding that can be exploited, by MRI, to develop an index of arterial wall lipid infiltration. The extent and location of increased vascular lipid infiltration can then be used to determine the presence of a lesion with an increased likelihood of subsequent clinical instability (i.e., a thin fibrous cap with increased luminal lipid deposition overlying a lipid-rich necrotic core). A self-contained intra-

From the \*Department of Vascular Surgery and Gottesdiener Vascular Biology Laboratory, The Sackler Faculty of Medicine, Tel Aviv University, Tel Aviv, Israel; †Cardiovascular Division, Hospital of the University of Pennsylvania, Philadelphia, Pennsylvania; ‡TopSpin Medical Israel, Lod, Israel; §Department of Cardiology Carmel Hospital, Haifa, Israel; ||Wolfson Hospital, Holon, Israel; and ¶Department of Cardiovascular Pathology, Armed Forces Institute of Pathology, Washington, DC. Drs. Schneiderman, Wilensky, and Virmani are consultants for Topspin Medical. A. Weiss, E. Samouha, L. Muchnik, M. Chen-Zion, M. Ilovitch, E. Golan, and A. Blank are employees of Topspin Medical.

Manuscript received July 7, 2004; revised manuscript received August 14, 2004, accepted September 21, 2004.

**Abbreviations and Acronyms**

- ADC = apparent diffusion coefficient
- DOV = depth of view
- FOV = field of view
- LF = lipid fraction
- MRI = magnetic resonance imaging
- SNR = signal to noise ratio
- TCFA = thin-cap fibroatheroma

vascular MRI probe was designed to obtain high-resolution MRI, thereby revealing the depth and size of the necrotic core and assess fibrous cap thickness. The current study was performed to evaluate the sensitivity and specificity of this novel intravascular MRI catheter for the detection of human aortic and coronary TCFA.

**METHODS**

**System description.** The intravascular MRI system (Top-Spin Medical Israel Inc., Lod, Israel) consists of a miniature self-contained MRI catheter and a portable control unit (Fig. 1). Magnetic fields generated by the probe located at the tip of the catheter create a sector-shaped sensitive region

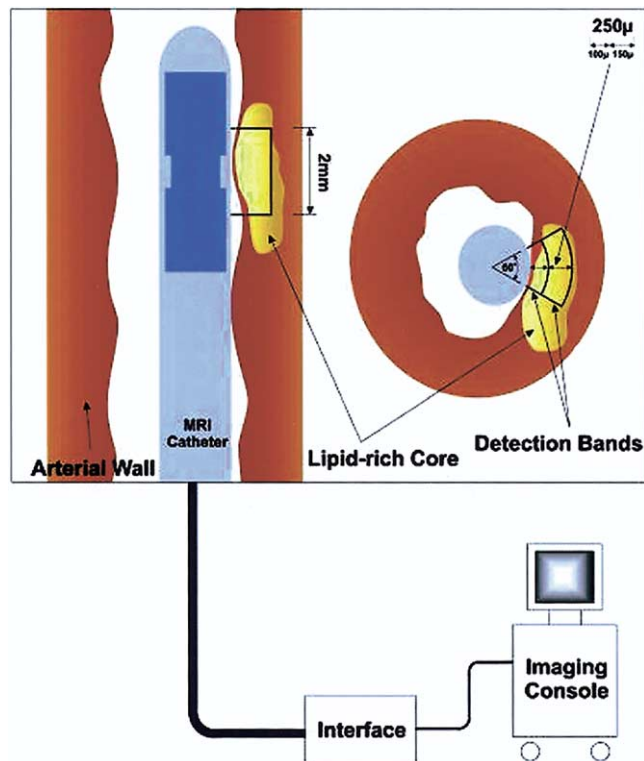


**Figure 1.** Schematic representation of the magnetic resonance imaging (MRI) catheter within an artery. (Left) The artery is shown in the longitudinal axis with juxtaposition of the MRI catheter close to a segment of the arterial wall containing a lipid-rich core. The slice thickness of the MRI measurement is 2 mm in length. (Right) Cross section of the artery is shown with the catheter in close proximity to a radial 60° section containing two evaluated detection bands within the field of view (0 to 100 μm and 100 to 250 μm). The catheter is connected to its interface control unit and the imaging console.

looking sideways into the artery wall. The MRI probe is characterized by very strong static local gradients in the imaging region, which ranges between 150 and 200 T/m (13).

The MRI catheter provided a depth of view (DOV) imaging in the radial (or *x*) plane of 250 μm, lateral resolution of a 60° sector, and slice thickness of 2 mm (Fig. 1). To achieve high-resolution imaging, the MRI catheter is stabilized against the arterial wall by gentle inflation of a partially occlusive side balloon. Although evaluation of arterial wall depth >250 μm is possible, the signal-to-noise ratio (SNR) for voxels >300 μm from the probe surface requires long averaging times (>90 s), which potentially prohibit such acquisitions within coronary arteries. In order to evaluate the thickness of the fibrous cap with regard to TCFA, magnetic resonance (MR) assessment is performed simultaneously in two separate bands: a superficial, luminal 0 to 100 μm band and a deeper 100 to 250 μm band. Physically speaking, the *x* plane resolution is <1 μm due to the high gradient. However, the particle resolution is limited by the SNR and the available acquisition time, so that the resolution in the present case is 100 μm.

Signal acquisition per sector requires ~40 s of averaging to obtain an appropriate SNR. The subsequent data readout is instantaneous. The acquisition time was ~2.5 to 4 min per sector to acquire detailed parametric data (actual *T<sub>c</sub>* or ADC), as opposed to simple diffusion-weighted signal averaging. Intraplague lipids have a very short *T<sub>2</sub>* that results in low SNR, and so the pulse sequence used was CPMG (Carr-Purcell-Meiboom-Gill) with an extremely short time between each echo in the train (denoted *T<sub>E</sub>*) of ~12 μs (14). This allows acquisition of more than a thousand echoes per single *T<sub>2</sub>* with accumulation of ~135,000 echoes over the 40-s averaging period and improves the single-shot SNR by a factor of ~365. In addition, the strong inherent static gradient created by the probe makes self-diffusion the most dominant factor in echo decay over the echo train.

**Magnetic resonance acquisition and data processing.** A water diffusion time constant was derived from the acquired MRI measurement by fitting the echo train to an exponential function using a previously described algorithm that calculates nuclear magnetic resonance signals of multi-echo pulse sequence with arbitrary position dependent *B<sub>0</sub>* and *B<sub>1</sub>* fields, taking into account relaxation and spin diffusion (15). The derived time constant relates specifically to the diffusion coefficient of the tissue and is the basis for the lipid fraction (LF) that represents the percentage of lipid within the evaluated volume. The term “lipid fraction” rather than lipid diffusion is used, as it is more intuitive to clinicians. In order to determine the lipid fraction of the arterial wall, MRI catheter measurements were performed in four quadrants (Fig. 2). Within each DOV, the percentage of lipid was assessed in each quadrant in both the superficial and deep bands simultaneously, and the data were integrated to produce a circular color-coded display (see subsequent text). The resulting image, therefore, represents the sum of the

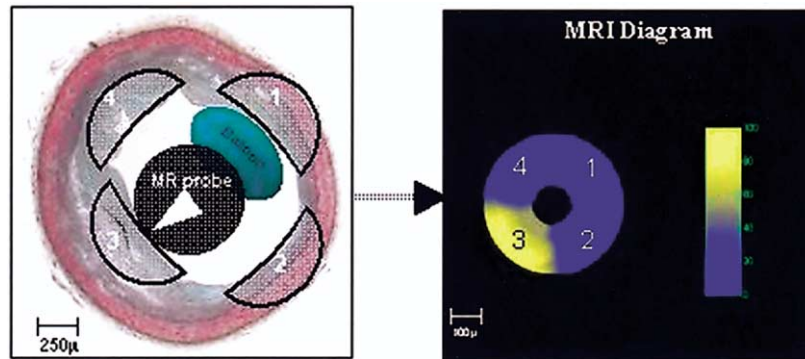


**Figure 2.** Depiction of the magnetic resonance imaging (MRI) catheter with imaging areas superimposed on a cross section of a human coronary artery (left). Interrogation of the arterial wall is in four quadrants, each comprising a field of view. A single field of view is denoted by the white arrowhead. The MRI diagram (right) displays the lipid fraction in each quadrant assessed by the catheter. In this particular illustration, an increased lipid concentration is noted only in quadrant 3, as it displays yellow. Quadrants 1, 2, and 4 are shown in blue, indicating a low lipid content or increased fibrous content.

four superficial and four deep field of view (FOV) bands from the four quadrants. The FOV defines the angular, longitudinal, and radial dimensions of the measured volume. The MRI determinants of TCFA were defined as the presence of an increased lipid fraction within the superficial band (0 to 100  $\mu$ ) of the arterial wall, which in turn denotes the presence of a thin fibrous cap, as well as increased lipid in the deep DOV, which indicates the presence of a necrotic core or an increased concentration of lipid-rich cells. Conversely, the absence of lipid within the superficial DOV indicates a thick fibrous cap, which is associated with more stable lesions. A sizeable necrotic core within the deep band associated with a shallow band devoid of lipid renders the diagnosis of a stable lesion or thick-cap fibroatheroma.

**Tissue selection.** Hearts and aortas were obtained within 8 to 12 h of death from 14 autopsy cases suspected of sudden coronary death. Unfixed tissues were initially assessed with postmortem fluoroscopy for the extent of calcium deposition. Sixteen segments from the proximal aortic arch were selected, representing a variety of noncalcified atherosclerotic lesions. All hearts were screened for coronary atherosclerosis by selective coronary angiography.

**Determination of lipid fraction index.** Fresh aortic samples were initially evaluated for the presence of atherosclerotic lesions. These samples were then separated into various plaque components to yield homogeneous arterial contents, including normal arterial tissue, fibrous tissue, foam cells, and necrotic cores. The following MRI parameters were used: mean gradient 175 T/m,  $T_1$  for lipid samples 200 ms and for fibrous samples 450 ms, infinite  $T_2$  with a  $T_E$  of 22  $\mu$ s to obtain the ADC using MR diffusion simulation previously published (15). The  $T_2$  value was set to infinity, as it has no significant effect on the diffusion, because self-diffusion is the most dominant factor in echo decay (see the previous text). By histopathology, two extremes, with regard to lipid content, were defined: a lipid-rich necrotic core was defined as 100% lipid fraction and a completely fibrous tissue specimen, and devoid of lipid was defined as 0%. A linear scale was then designed so that  $LF = (T_C [\text{measured}] - T_C [\text{fibrous}]) / (T_C [\text{necrotic core}] - T_C [\text{fi-$

brous tissue]) and designed to produce a read-out from blue to yellow such that pure blue corresponds to 0% LF and pure yellow to 100% LF.

**Aortic evaluation.** Samples collected from the aortic arch were highly variable in appearance and included specimens thought to represent a wide range of atherosclerosis: lipid-rich necrotic core lesions (i.e., ulcerated plaques, TFCAs, and thick-cap fibroatheromas), lesions with lipid pools and/or fatty streaks, and adaptive intimal hyperplasia. Selected rectangular segments were washed in saline, trimmed to 1 to 3 cm, mounted on a small tray, and immersed in a saline bath at 37°C. The MRI catheter was approximated sideways against the tissue facing the site of interest. After the acquisition period, the segment was tagged to denote the area of interrogation on the luminal surface. The tissues were then fixed in 4% formalin and processed for histology.

**Coronary study.** All 14 hearts underwent selective coronary angiography of the left and right coronary arteries. Of the 14 hearts, 7 had a total of 18 intermediate coronary lesions, ranging from 30% to 60% in diameter stenosis. The location of each lesion was marked on the epicardial surface, and the heart was then mounted within a conical saline bath warmed to 37°C. The MRI catheter was introduced through a guiding catheter placed in the coronary artery orifice and advanced into the lesion. Pulsatile saline flow at 37°C was generated within the coronary artery through the guiding catheter. The side balloon of the catheter was gently inflated to approximate the probe against the arterial surface, and MR measurement in one quadrant was obtained. The balloon was deflated and the probe rotated by using a manual rotation device in fixed increments of 90° to provide additional measurements. The circumferential orientation was confirmed using ink markers on the catheter. The exact longitudinal position was confirmed using a transmit loop antenna, which applies external radiofrequency (RF) energy to the arterial surface, allowing for precise localization of the MRI receiving coil within the ex vivo artery. Measurements at four quadrants were performed in most instances (in total, 68 measurements in the 18 lesions). Immediately after MRI evaluation, the

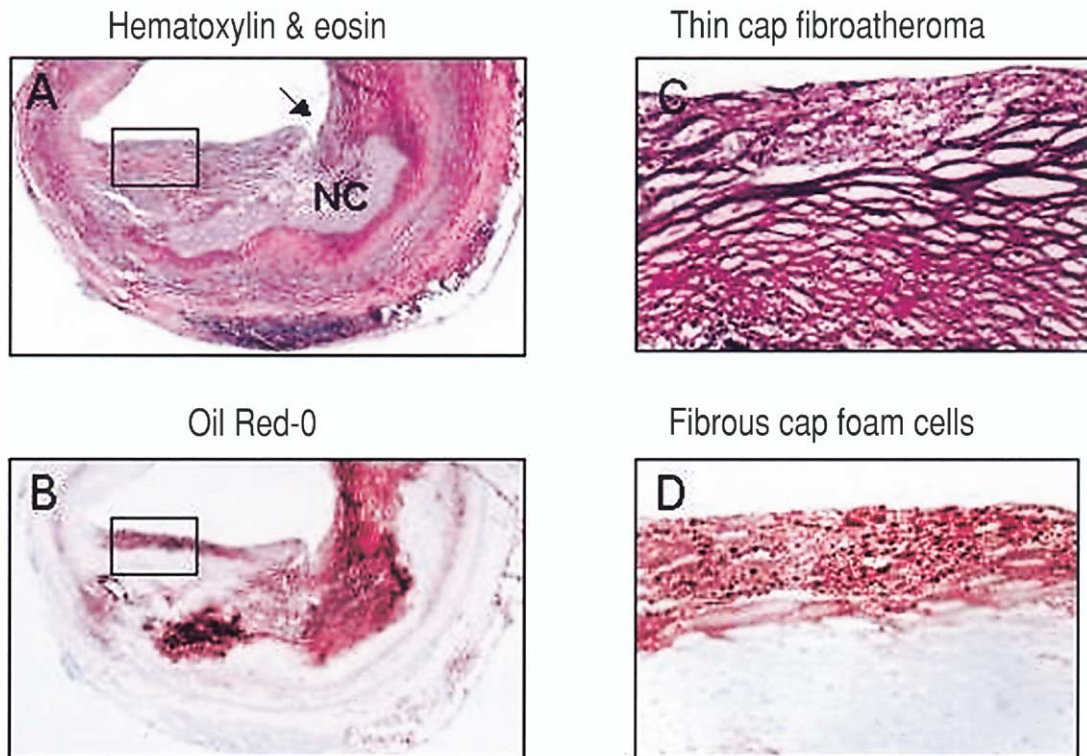


**Figure 3.** Photomicrographs of a thin cap fibroatheroma in a human coronary artery. (A) An old rupture of the fibrous cap overlying a large necrotic core (NC) is shown (arrow) (section stained with hematoxylin-eosin). (B) Adjacent section stained with oil red O to demonstrate the presence of lipids within the arterial wall. Note that increased staining is noted throughout the lesion both in the area of the NC as well as the fibrous cap (box). (C, D) Higher magnifications of boxed areas seen in A and B. Panel C shows foam cells within the thin fibrous cap stained with hematoxylin-eosin, whereas panel D shows oil red O staining. This artery was correctly identified as a thin cap fibroatheroma by magnetic resonance imaging.

examined arteries were removed and arterial segments 3 to 4 mm length containing the interrogated lesion were processed for histologic evaluation.

**Histopathologic analyses.** Arterial segments were fixed in 4% formalin for 8 to 12 h, embedded in paraffin, and serially sectioned at 5 to 6  $\mu$  intervals through the area of interest. Sections 100  $\mu$  apart were stained with hematoxylin-eosin and Movat's pentachrome stains. The presence of macrophages was determined by immunohistochemical staining for CD-68. Staining with oil red O was used to document the presence of lipid within the arterial wall within foam cells, cholesterol crystals, and necrotic core (Fig. 3). Lesions on the Movat pentachrome sections were then catalogued according to the recently published classification (4). The TFCAs (vulnerable plaques) were defined as lesions containing necrotic cores covered by thin (<75  $\mu$ m) fibrous caps. The presence of any portion of the sector of the coronary artery containing an area of fibrous cap <75  $\mu$ m in thickness was sufficient to classify that arterial segment as TFCA. Fatty streaks (intimal xanthomas) were lesions abundant with foam cells, regardless of fibrous cap thickness. Thick-cap fibroatheromas had a necrotic core, but fibrous caps >75  $\mu$  thick. Fibrocalcific lesions contained few foam cells and no necrotic cores but were predominantly fibrous with or without calcification. Adaptive intimal thickening was tissue rich in proteoglycans and collagen and

smooth muscle cells without foam cells or necrotic core. Histologic results were compared with MRI results.

**Statistical analysis.** Numerical data are presented as the mean value  $\pm$  SD, unless otherwise noted. An unpaired *t* test was used to determine significant difference, and a *p* value of <0.05 was considered statistically significant.

## RESULTS

**Determination of lipid fraction index.** Significant differences in ADC between fibrous tissue (or fibrous cap), fatty streak, and lipid-rich necrotic core (intact or ruptured) were demonstrated (Table 1). Further studies on aortic samples demonstrated that the MRI measurement at any site within each band demonstrated increased LF values in lesions designated by histology (Fig. 4) as containing a necrotic core (n = 13, LF index:  $69 \pm 14\%$ ) and foam cells (n = 7, LF index:  $46 \pm 12\%$ ; *p* < 0.001 vs. necrotic core), compared with fibrous tissue (n = 11, LF index:  $13 \pm 13\%$ ; *p* < 0.0001 vs. necrotic core).

**Aortas.** Sixteen aortic specimens, representing a wide range of lesion types, were diagnosed as follows: ulcerated plaques (absence of fibrous cap, n = 4), TCFAs (n = 2), thick-cap fibroatheromas (n = 2), intimal xanthomas (n = 2), and adaptive intimal thickening (n = 6). Data derived from the MRI catheter correlated to histology in 15 (94%) of 16

**Table 1.** Apparent Diffusion Coefficients of Lipid-Rich and Fibrotic Tissues Obtained From Homogenous Aortic Samples Representing the Extreme Tissue Type for 100% and 0% Lipid Concentration, Respectively

	ADC (m <sup>2</sup> /s)	T <sub>c</sub> (ms)*		Lipid Fraction (%)	
		100 μm	250 μm	100 μm	250 μm
Lipid rich necrotic core	0.4E-9	14.2	15.7	100	100
Fibrous/SMC	1.6E-9	4.9	4.0	0	0

\*Extremes T<sub>c</sub> values were taken as the mean value + 1 standard deviation in case of lipid and mean value - 1 standard deviation in case of fibrous (± error for 95% confidence level).

ADC = apparent diffusion coefficients; SMC = smooth muscle cell.

cases. One thick-cap fibroatheroma was misdiagnosed as TCFA by MRI. Examples are shown in Figure 5.

**Coronary arteries.** The MRI diagnosis of lesion characteristics correlated with histologic diagnosis in 16 (89%) of 18 lesions. Lesions were classified as adaptive intimal thickening (n = 1), fatty streak (intimal xanthoma, n = 2), thick-cap fibroatheroma (n = 4), TCFA (vulnerable plaque, n = 3; Fig. 3), ruptured plaque with intraplaque hemorrhage (n = 1), plaque hemorrhage (n = 1), healed plaque rupture (n = 1), and fibrocalcific plaque (n = 5). The MRI diagnosis for every specimen was obtained by integrating lipid fraction data, which was assessed within both bands simultaneously, within each quadrant. Individual results are shown in Table 2. Examples are shown in Figure 6. Results of histology in addition to the aortic data resulted in a sensitivity of 100% and a specificity of 89%.

## DISCUSSION

This study was performed to evaluate the diagnostic capabilities of a novel, self-contained intravascular MRI catheter system to document the presence of atherosclerotic lesions within human coronary arteries and aortae that possess increased intramural lipid. We elected to interrogate intermediate coronary stenoses, as these are the most likely

to undergo transformation into an unstable lesion. Such vulnerable lesions often do not exhibit hemodynamic significance but may possess an increased lipid content and macrophage count, making them more susceptible to rupture (16,17). The results demonstrate the potential feasibility of the intravascular MRI catheter in interrogating lesions possessing a large lipid core, thin fibrous cap, and increased macrophage infiltration—hallmarks of a potentially unstable plaque. In addition, analysis of aortic lesion composition demonstrated the ability of the MRI catheter to distinguish between necrotic core, foam cells, and fibrous tissue based on the tissue's lipid fraction. Hence, discrimination can be made between early atherosclerotic lesions containing primarily foam cells and advanced, potentially vulnerable lesions with relatively large necrotic cores.

Coronary lesions with the propensity of rupture or erosion resulting in acute thrombosis represent the underlying pathophysiologic substrate of acute coronary syndromes. These lesions are frequently <50% in angiographic severity before clinical presentation (2,18-21). Although the diagnosis of vulnerable lesions is made on necropsy, there are examples in which invasive methods of coronary lesion appearance correlated with subsequent clinical events. Uchida et al. (22), using coronary angiography in patients

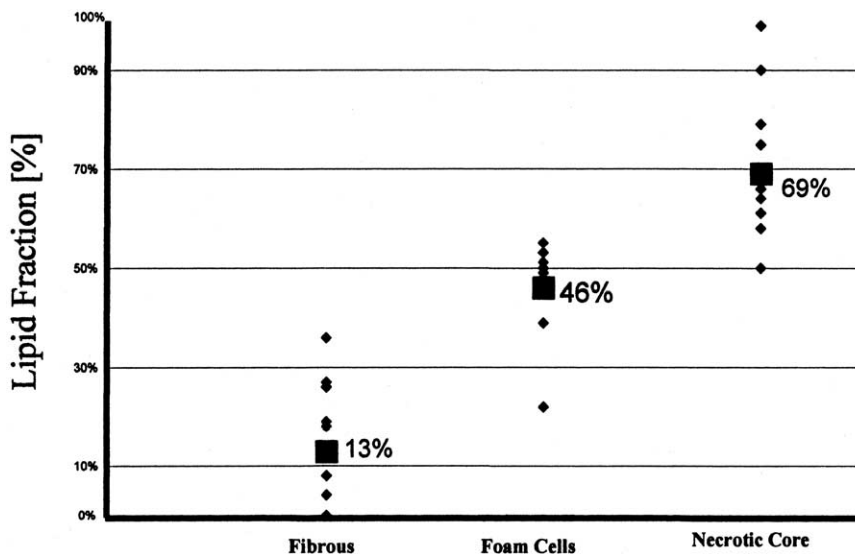


**Figure 4.** Lipid fraction assessed by magnetic resonance imaging in three homogeneous components of aortic atherosclerotic lesions. The fibrous component showed the least amount of lipid (13 ± 13%), significantly less than that obtained from areas rich in foam cells (46 ± 12%, p < 0.0001) and necrotic cores (69 ± 14%, p < 0.0001 vs. fibrous plaque, p < 0.001 vs. foam cells).

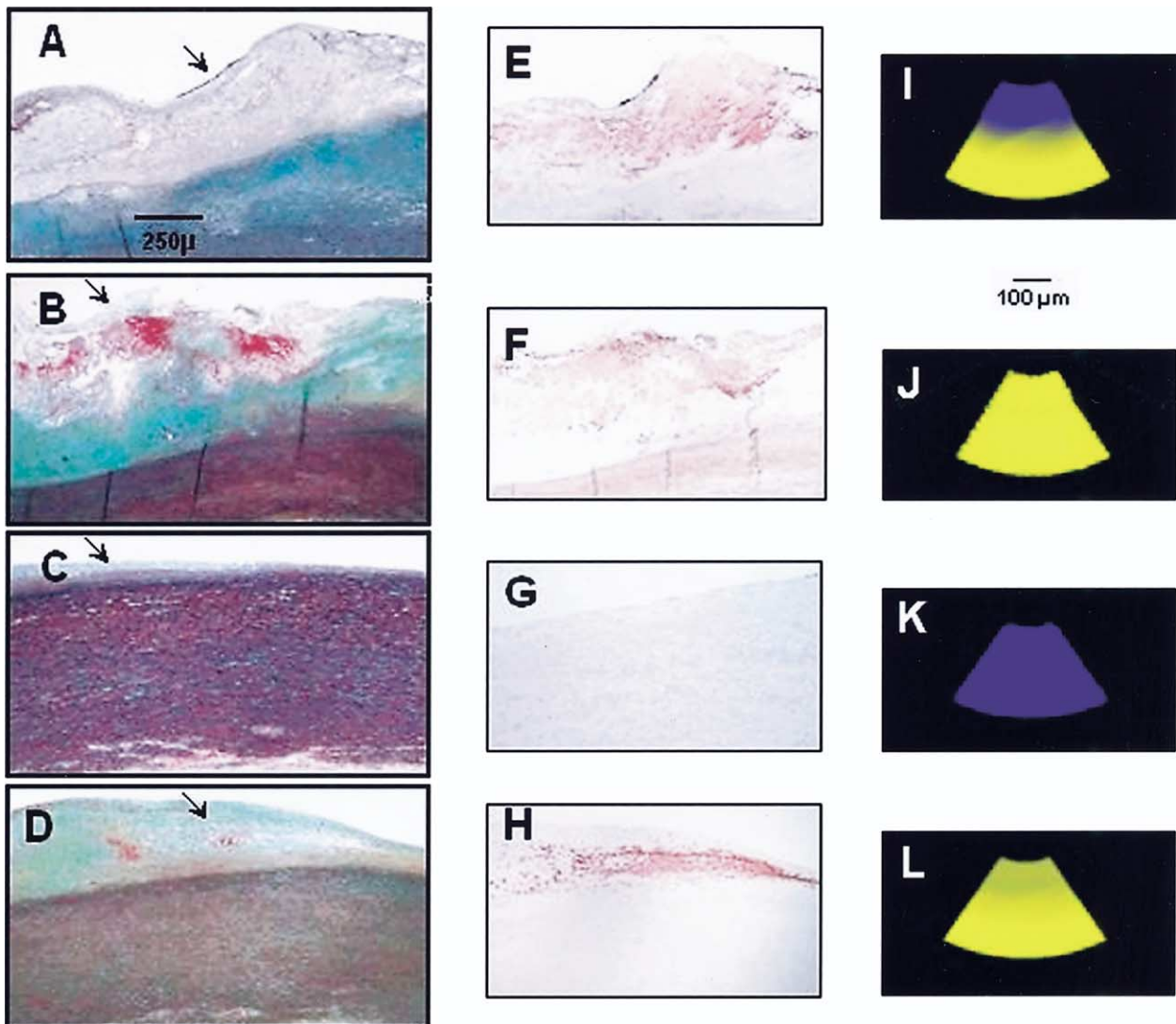


**Figure 5.** Examples of four aortic specimens and corresponding MRI displays. (A to D) Movat's pentachrome-stained samples. (E to H) Adjacent sections stained with anti-CD-68 (brown) to identify areas rich in macrophages and lipid. (I to L) Corresponding intravascular magnetic resonance imaging (MRI) displays. Arrows indicate the location of MRI interrogation. (A, E) Thick-cap fibroatheroma with the fibrous cap at the site of MRI measurement ~120  $\mu\text{m}$  in thickness (arrow). The CD-68 photomicrograph (E) reveals that an increased macrophage concentration is observed primarily in the deep layer. The corresponding MRI display (I) demonstrates the presence of lipid in the 100 to 250  $\mu\text{m}$  deep layer (yellow), whereas the superficial 0 to 100  $\mu\text{m}$  segment has a low lipid content, thus the MRI read-out is blue. (B, F) Ulcerated plaque; the interrogated necrotic core is near the surface (arrow). There are hemorrhagic areas within the necrotic core, and the corresponding CD-68-stained section (F) shows increased staining in the necrotic core. The corresponding MRI display indicates a high lipid content in both the superficial and deep bands (0 to 100  $\mu\text{m}$  and 100 to 250  $\mu\text{m}$ ). (C, G) Normal aortic wall devoid of plaque. No anti-CD-68 staining is observed in panel G. The MRI interrogation (K) showed a high fibrous content and is devoid of lipid (blue) in both bands. (D, H) Thin-cap fibroatheroma (cap ~50  $\mu\text{m}$  in thickness) with the cap infiltrated by foam cells and a deeper necrotic core observed in the histologic section, as well as in the corresponding CD-68-stained section (H). The MRI display shows a high lipid content within both bands (L). Original magnification is  $\times 20$ . The 100- $\mu\text{m}$  bar is for the MRI images, whereas the 250- $\mu\text{m}$  bar is for the Movat's and CD-68-stained sections.

with stable angina, demonstrated that glistening yellow lesions, thought to reflect increased underlying lipid content, were more likely to have an acute coronary event in the subsequent year, compared with white lesions. Approximately two-thirds of the lesions that ruptured did so within two months. Yamagishi *et al.* (23) used intravascular ultrasound to identify lesions with superficial echolucent areas, thought to represent necrotic cores in patients with stable and unstable angina. Of the 12 patients who had an acute coronary syndrome during the two-year follow-up, 10 had echolucent areas (83%) on the initial study, versus only 19

(21%) of 90 patients without a subsequent acute coronary syndrome.

The approach presented in this report is novel and differs fundamentally from conventional MRI with or without intravascular coils. Conventional MRI techniques are based on creating the magnetic fields (static, gradient, and RF) from outside the patient. The highly homogeneous fields and the linear gradients created by such an approach allow for acquisition of large FOV images. Using intravascular reception coils improves the SNR obtained in the immediate surroundings of the coil, whereas other aspects of MRI

**Table 2.** Correlation of MRI Diagnosis and Histopathology in Intermediate Coronary Lesions

Lesion #	MRI		
	Analysis in Quadrants	Diagnosis	Histopathology Diagnosis
1	AA, BA, AB, AA	Non-VP	Fatty streak
2	CC, CB, AA, CA	TFCA	TFCA
3	BA, AA	Non-VP	Fibrous cap atheroma
4	CC, CB, CA, BA	TCFA	TFCA
5	AA, AB	Non-VP	Fibrous cap atheroma
6	BA, BA, AA, BA	Non-VP	Fibrous cap atheroma
7	BB, AA, AA, CA	Non-VP	Fibrous cap atheroma
8	AA, AA, BA, AB	Non-VP	Fibrocalcific plaque
9	AA, AB, AA, AA	Non-VP	Fibrocalcific plaque
10	AB, BB, AA, AC	Non-VP	Fibrocalcific plaque
11	CC, BA, AA, AB	TCFA	Fibrocalcific plaque
12	AA, AA, BB, CC	TCFA	Fibrocalcific plaque
13	BA, AC, CC, BA	TCFA	TFCA
14	AA, AB, BA, BB	Non-VP	Ruptured plaque with hemorrhage
15	AC, AA	Non-VP	Fatty streak
16	AA, AA, BB, BB	Non-VP	Healed plaque rupture
17	AA, AB	Non-VP	Plaque hemorrhage
18	AA, AA, AA, AA	Non-VP	Adaptive intimal thickening

Note: The letters in the MRI analysis column symbolize MRI tissue diagnosis, as follows: A = fibrous tissue; B = foam cells; C = necrotic core. Each letter pair (i.e., AA) represents a quadrant; whereby, the first letter represents the 0 to 100  $\mu$ m band (luminal) and the second letter the 100 to 250  $\mu$ m band. In four lesions MRI analysis was performed in two quadrants only 180° apart. Thin-cap fibroatheroma (vulnerable plaque) has been defined as CC or BC in at least one of the measured quadrants.

MRI = magnetic resonance imaging; TCFA = thin-cap fibroatheroma; VP = vulnerable plaque.

remain the same (e.g., image coordinates, contrast methods). However, the use of external magnets and field sources results in two fundamental limitations of conventional techniques: relative motion of coronary arteries with respect to gradient fields does not allow for continuous signal integration and limits the in-slice spatial resolution. This poses a significant limitation in imaging of small necrotic cores in coronary arteries. In addition, using large and expensive MRI scanners in dedicated MRI laboratories limits their use in interventional procedures. These limitations are not present in the intravascular MRI catheter system. Furthermore, given the effective approximation of the catheter to the vessel wall, gating techniques to ensure adequate image acquisition are unnecessary.

Intravascular MRI using this probe is not a reflection of the actual morphology of the plaque but provides a simplified spatial representation of its lipid-rich component. The probe cannot differentiate between the fibrous cap and the normal medial layer using the current pulse sequence. This is not unexpected, as Toussaint et al. (12) showed that the fibrous cap and normal arterial media possess similar biophysical constraints, and hence, similar water diffusion coefficients. The core of an atheromatous intermediate lesion has no confining structures and water diffuses isotropically, allowing differentiation of the lipid core from the fibrous cap and the normal medial layer. Differentiation of the fibrous cap and the normal medial layer is not considered clinically important in determining the vulnerability of an arterial lesion (Fig. 6B, quadrant 5).

The limitations of the current MRI catheter are its size (6-F) and the need to compromise coronary blood flow during catheter stabilization with balloon inflation and to

mechanically rotate the catheter to achieve circumferential sector assessment of the arterial wall. Current catheter developments have reduced the catheter size to 5.2-F. The presented catheter configuration provides a DOV of 250  $\mu$ m and a lateral resolution of 60°. Hence, to obtain a circumferential study per tissue slice, it was necessary to perform separate measurements in four quadrants along the arterial circumference. Because the catheter is designed to be effective in intermediate lesions with arterial luminal diameters ranging from 2 to 3 mm, each 60° sector interrogates a circumferential arc of ~1 mm. For 2- to 3-mm diameter arteries, one would expect interrogation of 4 mm of the 6- to 9-mm circumference, which is equal to 67% of the circumference of a 2-mm artery and 45% of a 3-mm artery. This extent of interrogation may be sufficient to identify TCFA in vivo, as recent histopathologic data evaluating the circumferential distribution of the necrotic core of TCFA have shown that vulnerable plaques have an angular span of at least 120° in over 75% of the cases (24).

An important limitation of all techniques evaluating potential vulnerable plaques is that current knowledge is based on pathologic studies showing that coronary instability may be caused by either rupture of TFCA or plaque erosion. Whether any technique, including intravascular MRI, can document the presence of both pathologic subsets is unknown and awaits prospective clinical studies. Likewise, the validity of determining the exact location of a TCFA in order to prophylactically reduce coronary death or myocardial infarction must be tested in a randomized, prospective clinical trial.

**Conclusions.** Miniaturization of MRI capabilities into the intravascular catheter, free of external magnets or

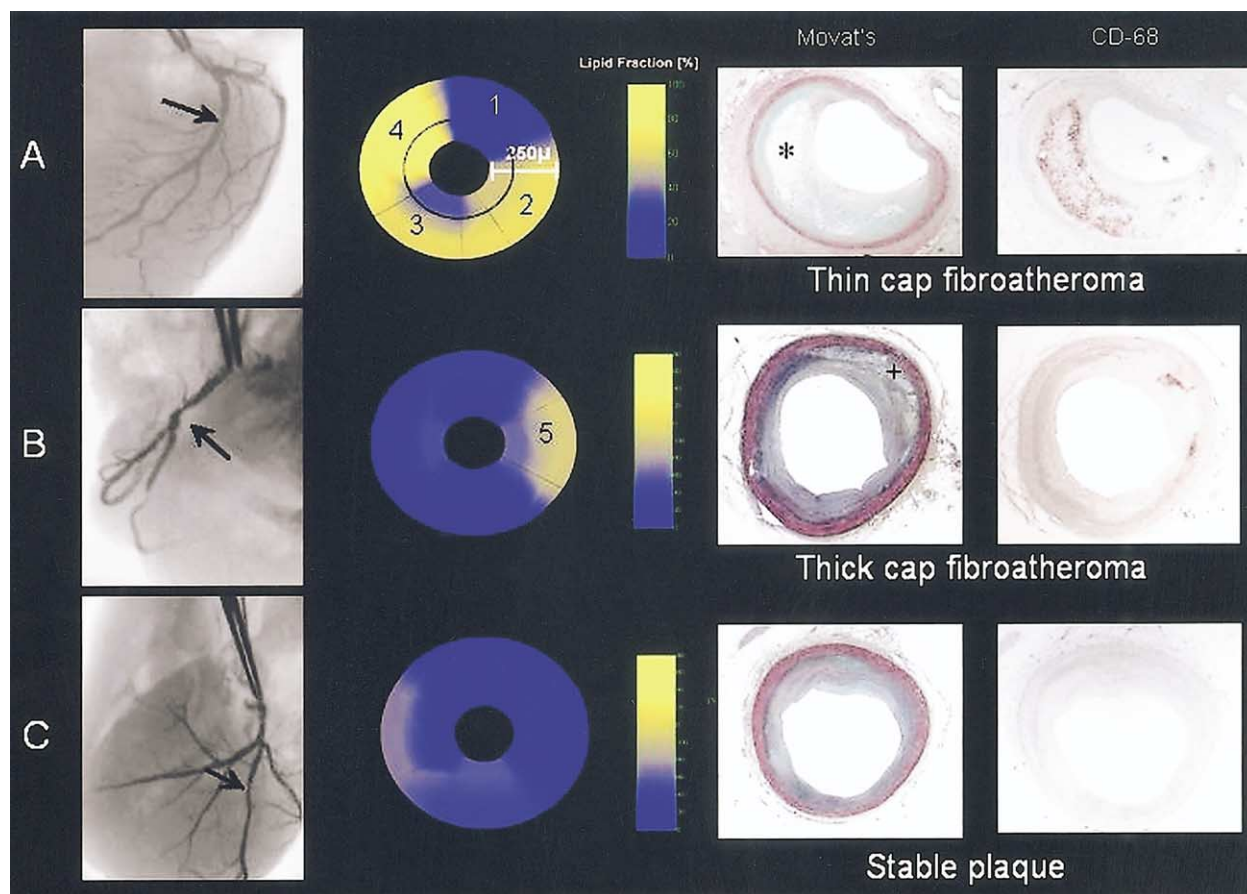


**Figure 6.** The magnetic resonance imaging (MRI) scan demonstrates excellent correlation with histology. Coronary angiography, MRI, and histologic cross sections of three intermediate coronary lesions are shown. An **arrow** on the angiogram marks the site of interrogation. The corresponding MRI is shown in the second column, whereas corresponding histologic sections of the interrogated sections are shown in the third and fourth columns (Movat's pentachrome and anti-CD-68 antibody staining, respectively). **(A)** Thin-cap fibroatheroma (**left to right**) in the proximal left anterior descending artery; the MRI display shows the presence of a high lipid content within three quadrants (2 to 4). Quadrant 1 has little lipid within the wall, as indicated by the lack of foam cells by Movat's staining or macrophages by CD-68 staining. Quadrant 2 has moderately increased lipid concentrations, as noted by an approximate lipid fractional index of 60%. Quadrant 3 has increased lipid only in the deep layer, whereas quadrant 4 has high lipid fractional indexes ( $\pm 100\%$ ) within the superficial and deep layers. Approximately 75% of the arterial circumference is lipid-rich. The MRI display corresponds well with subsequent histology, as the Movat's section shows a large necrotic core (\*) and a thin fibrous cap, and the adjoining immunohistochemical staining shows markedly positive staining for CD-68 in the area corresponding to quadrant 4 of the MRI display. **(B)** Thick-cap fibroatheroma in the right coronary artery. The MRI display shows no lipid content within the superficial layer (**blue**); however, a mild degree of increased lipid concentration is observed within the deep band ( $>100 \mu\text{m}$  from the lumen in quadrant 5 only). The lipid fractional index is about 50%. The corresponding histologic section shows a thick-cap fibroatheroma with a small, deep necrotic core (+), confirmed by the anti-CD-68 staining, corresponding with the MRI image. Because there is little to no lipid within the superficial layer, this lesion is considered a thick fibroatheroma. **(C)** Stable lesion. A mild stenosis by angiography is seen in the intermediate branch of the left coronary artery. The MRI display of the lesion shows no increased lipid concentration in the shallow or the deep bands of any quadrant, indicating the presence of a fibrous lesion (hence, **blue** display). This diagnosis was confirmed by histology as adaptive intimal hyperplasia, and the corresponding anti-CD-68 staining was negative for foam cells or a necrotic core.

coils, may make coronary artery assessment of potentially vulnerable, intermediate lesions feasible in clinical practice. Reliable assessment of intermediate lesions may provide important data on the composition of the atherosclerotic lesion, thereby predicting the likelihood of eventual rupture and clinical instability and allowing guidance of local treatment.

**Reprint requests and correspondence:** Dr. Robert L. Wilensky, Hospital of the University of Pennsylvania, 3400 Spruce Street, 9 Gates, Philadelphia, Pennsylvania 19104. E-mail: Robert.Wilensky@uphs.upenn.edu.

## REFERENCES

1. Fuster V, Badimon L, Badimon JJ, Chesebro JH. The pathogenesis of coronary artery disease and the acute coronary syndromes (2). *N Engl J Med* 1992;326:310-8.
2. Falk E, Shah PK, Fuster V. Coronary plaque disruption. *Circulation* 1995;92:657-71.
3. Libby P. Coronary artery injury and the biology of atherosclerosis: inflammation, thrombosis, and stabilization (with discussion). *Am J Cardiol* 2000;86:3-9J.
4. Virmani R, Kolodgie FD, Burke AP, Farb A, Schwartz SM. Lessons from sudden coronary death: a comprehensive morphological classification scheme for atherosclerotic lesions. *Arterioscler Thromb Vasc Biol* 2000;20:1262-75.
5. Kereiakes DJ. The Emperor's clothes: in search of the vulnerable plaque. *Circulation* 2003;107:2076-7.

6. Monroe VS, Kerensky RA, Rivera E, Smith KM, Pepine CJ. Pharmacologic plaque passivation for the reduction of recurrent cardiac events in acute coronary syndromes. *J Am Coll Cardiol* 2003;41:S23-30.
7. Shah PK. Mechanisms of plaque vulnerability and rupture. *J Am Coll Cardiol* 2003;41:S15-22.
8. Maseri A, Fuster V. Is there a vulnerable plaque? *Circulation* 2003;107:2068-71.
9. Casscells W, Naghavi M, Willerson JT. Vulnerable atherosclerotic plaque: a multifocal disease. *Circulation* 2003;107:2072-5.
10. Yuan C, Zhang SX, Polissar NL, et al. Identification of fibrous cap rupture with magnetic resonance imaging is highly associated with recent transient ischemic attack or stroke. *Circulation* 2002;105:181-5.
11. Fayad ZA, Fuster V. Characterization of atherosclerotic plaques by magnetic resonance imaging. *Ann NY Acad Sci* 2000;902:173-86.
12. Toussaint JF, Southern JF, Fuster V, Kantor HL. Water diffusion properties of human atherosclerosis and thrombosis measured by pulse field gradient nuclear magnetic resonance. *Arterioscler Thromb Vasc Biol* 1997;17:542-6.
13. Blank A, Alexandrowicz G, Muchnik L, et al. Miniature self-contained NMR probe for clinical applications. *Magn Res Med* 2005. In press.
14. Meiboom S, Gill D. Modified spin-echo method for measuring nuclear relaxation times: review of scientific instruments. 1958;29:688-691.
15. Zur Y. An algorithm to calculate the NMR signal of a multi spin-echo sequence with relaxation and spin-diffusion. *J Magn Res* 2004;17:97-106.
16. Pasterkamp G, Schoneveld AH, van der Wal AC, et al. Relation of arterial geometry to luminal narrowing and histologic markers for plaque vulnerability: the remodeling paradox. *J Am Coll Cardiol* 1998;32:655-62.
17. Varnava AM, Mills PG, Davies MJ. Relationship between coronary artery remodeling and plaque vulnerability. *Circulation* 2002;105:939-43.
18. Brown BG, Gallery CA, Badger RS, et al. Incomplete lysis of thrombus in the moderate underlying atherosclerotic lesion during intracoronary infusion of streptokinase for acute myocardial infarction: quantitative angiographic observations. *Circulation* 1986;73:653-61.
19. Ambrose JA, Tannenbaum MA, Alexopoulos D, et al. Angiographic progression of coronary artery disease and the development of myocardial infarction. *J Am Coll Cardiol* 1988;12:56-62.
20. Little WC, Constantinescu M, Applegate RJ, et al. Can coronary angiography predict the site of a subsequent myocardial infarction in patients with mild-to-moderate coronary artery disease? *Circulation* 1988;78:1157-66.
21. Alderman EL, Corley SD, Fisher LD, et al., the CASS Participating Investigators and Staff. Five-year angiographic follow-up of factors associated with progression of coronary artery disease in the Coronary Artery Surgery Study (CASS). *J Am Coll Cardiol* 1993;22:1141-54.
22. Uchida Y, Nakamura F, Tomaru T, et al. Prediction of acute coronary syndromes by percutaneous coronary angiography in patients with stable angina. *Am Heart J* 1995;130:195-203.
23. Yamagishi M, Terashima M, Awano K, et al. Morphology of vulnerable coronary plaque: insights from follow-up of patients examined by intravascular ultrasound before an acute coronary syndrome. *J Am Coll Cardiol* 2000;35:106-11.
24. Virmani R, Burke AP, Kolodgie FD, Farb A. Understanding atherosclerotic coronary artery disease: what makes the plaque unstable? Proceedings of the Paris Course on Revascularization (Euro PCR 04). 2004:7-32.